Journal of Power Sources 205 (2012) 264–271

Contents lists available at SciVerse ScienceDirect

Journal of Power Sources

journal homepage: www.elsevier.com/locate/jpowsour

Electrooxidation of ethanol on carbon-supported Pt–Pd nanoparticles

Jakub Seweryn, Adam Lewera*

Department of Chemistry, University of Warsaw, ul. Pasteura 1, 02-093 Warsaw, Poland

ARTICLE INFO

Article history:
Received 12 October 2011
Received in revised form
27 December 2011
Accepted 30 December 2011
Available online 9 January 2012

Keywords:
Platinum
Palladium
Ethanol electrooxidation
Direct ethanol fuel cells
Bi-functional mechanism

ABSTRACT

Carbon supported Pt–Pd nanoparticles with varying Pt content have been investigated as anodes in direct ethanol fuel cell. To gain insight on possible changes in the mechanism of electrooxidation of ethanol on Pt when it is alloyed with Pd, the products' yield have been determined as a function of cell voltage and anode composition in combination with ex situ electrochemical experiments. It has been determined that ethanol electrooxidation current density decreased almost linearly as Pd amount increased, with small local maximum imposed on the linear activity plot for nanoparticles with 1:1 Pt:Pd ratio. This maximum has been correlated to increased acetic acid production, which was the result of so-called bi-functional mechanism. The relative amount of acetic acid has been found to be inversely proportional to amount of CO_2 produced in wide range of conditions, where production of acetaldehyde was not correlated with production of other products. This observation was explained based on the possible paths of ethanol electrooxidation and competition between the adsorbed species for catalyst's surface. Overall the complex response of the system investigated can be understood in terms of interplay between bi-functional mechanism and ensemble effect and the electronic effects, albeit small, cannot be completely excluded.

1. Introduction

Low temperature fuel cells are considered as promising candidates for new sources of energy due to their high theoretical efficiency [1–3]. To achieve the high efficiency in practice, Pt-based catalysts are commonly used [1–17]. Hydrogen/oxygen, low temperature fuel cell with polymer electrolyte membrane is an example of such system, but its main drawbacks are: (i) the cost of anode and cathode catalysts and (ii) cost, storage and handling of hydrogen [1]. To overcome the drawbacks of hydrogen's use, liquid fuels are considered, such as methanol [2,3,5,18], ethanol [2,18–20], formic acid [20] and other small organic molecules [5,19]. In practice, for any liquid fuel, no sufficiently active anode catalyst is known as of today [2,3,13].

In search for more active catalysts many studies have been performed. It is known that Pt is very active material in application as anode, as well as cathode catalyst, but it is easily poisoned by the by-products of oxidation of organic molecules, such as carbon monoxide [8,10,21,22]. It has been shown, that bi-metallic catalysts containing Pt can be more active as anode catalysts than Pt alone, due to so-called bi-functional mechanism [21]. In that mechanism oxidation occurs on Pt sites, but the additional metal (i.e. Ru) can activate water and provide surface OH groups, which in turn are able to oxidize strongly adsorbed CO to CO_2 and free the Pt surface [21]. Many different bi- and tri-metallic systems were tested [4,6–9,11,15–17,21,23–28], and it has been determined, that in acid media Pt–Ru alloy is the most active toward oxidation of methanol [8,9,21], where Pt–Sn is the most active toward ethanol electrooxidation [4,6–9,11,15,24].

The analysis of product of ethanol electrooxidation revealed that the main products are acetaldehyde, acetic acid and CO_2 [10,14,23,24,29–35]. Those are products of 2, 4 or 12-electron oxidation of ethanol molecule, respectively [22,24,29,36]. Qualitative analysis of product of ethanol oxidation revealed that the most active catalysts in fact are able to increase the yield of acetic acid, which is in agreement with the bi-functional mechanism. It is worth to note, that acetic acid is effectively a dead end, as it cannot be further oxidized under the conditions of working fuel cell [29]. But there is no method to separate the chemical (bi-functional) enhancement of Pt–Sn and Pt–Ru activity toward electrooxidation of ethanol, from other factors (electronic, and structural), which may possibly play a role in observed enhancement.

Another interesting aspect is that in all systems currently investigated, except the tri-metallic systems containing Rh [16,17], enhancement in activity is not correlated with increased yield of CO_2, as compared to Pt alone [10,14]. Actually for Pt–Ru and Pt–Sn systems it is known, that the production of CO_2 significantly decreases, as compared to Pt [31,37,38]. Thus there is a need to find other materials, which are able to break C—C bond in ethanol.

* Corresponding author. Tel.: +48 22 822 0211x524; fax: +48 22 822 0211x524.
E-mail address: alewera@chem.uw.edu.pl (A. Lewera).

0378-7753/$ – see front matter © 2012 Elsevier B.V. All rights reserved.
doi:10.1016/j.jpowsour.2011.12.058

In order to design new catalysts the properties of Pt and Pt-containing systems needs to be better understood. The reason why Pt is able to break C—C bond to higher degree than its alloys (except tri-metallic systems containing Rh [16,17]) is still unclear. It has been suggested that electronic properties of platinum and the surface composition play significant role, to allow for activation of C—C bond due to preferential adsorption of ethanol molecule [2,39]. For this reason it is required to better understand how those properties change when Pt is alloyed.

We chose Pd as a second component of alloys with Pt, as it does not significantly enhance the catalytic activity of platinum toward ethanol electrooxidation. Inactivity of palladium toward ethanol electrooxidation is well established, resulting from the fact that ethanol does not adsorb on palladium [7,15,40]. It is generally not possible to analyze the changes in catalytic activity due to electronic and structural changes, resulting from alloying, when second component of the alloy is active toward ethanol, or facilitate its oxidation indirectly, i.e. via bi-functional mechanism. This exclude the use of Sn or Ru, the most common systems used as catalysts toward ethanol electrooxidation, and make Pd an attractive candidate for those studies.

Use of Pd was also dictated by the fact, that it is the element most similar to Pt in terms of crystal structure (identical – fcc), atomic size (only 3% of difference) and its ability to form alloys with Pt in whole range of composition. This allowed us to fine tune the composition of the resulting alloys. Compared to Pd, Ru and Sn have different crystallographic structures (hexagonal close packed and tetragonal, respectively for Ru and Sn, as compared to cubic close packed for Pt) and Pt–Sn forms intermetallic compounds (characterized by phases of discrete compositions). Such properties make Pd most suitable and allowed us to address the changes of catalytic activity, possible changes in ethanol electrooxidation mechanism (leading to different products) and possible electronic factors as an exclusive function of composition.

Here we used Pt–Pd alloys as model systems for both, electrochemical and fuel cell experiments, which combined allowed for better understanding of electrochemical oxidation mechanism of ethanol, which is of great importance for design and synthesis of new, more active catalysts for direct ethanol fuel cells. It is also worth to note that for some conditions, the decrease of activity is smaller than could be expected based on composition, and this study could also help to explain such behavior [41].

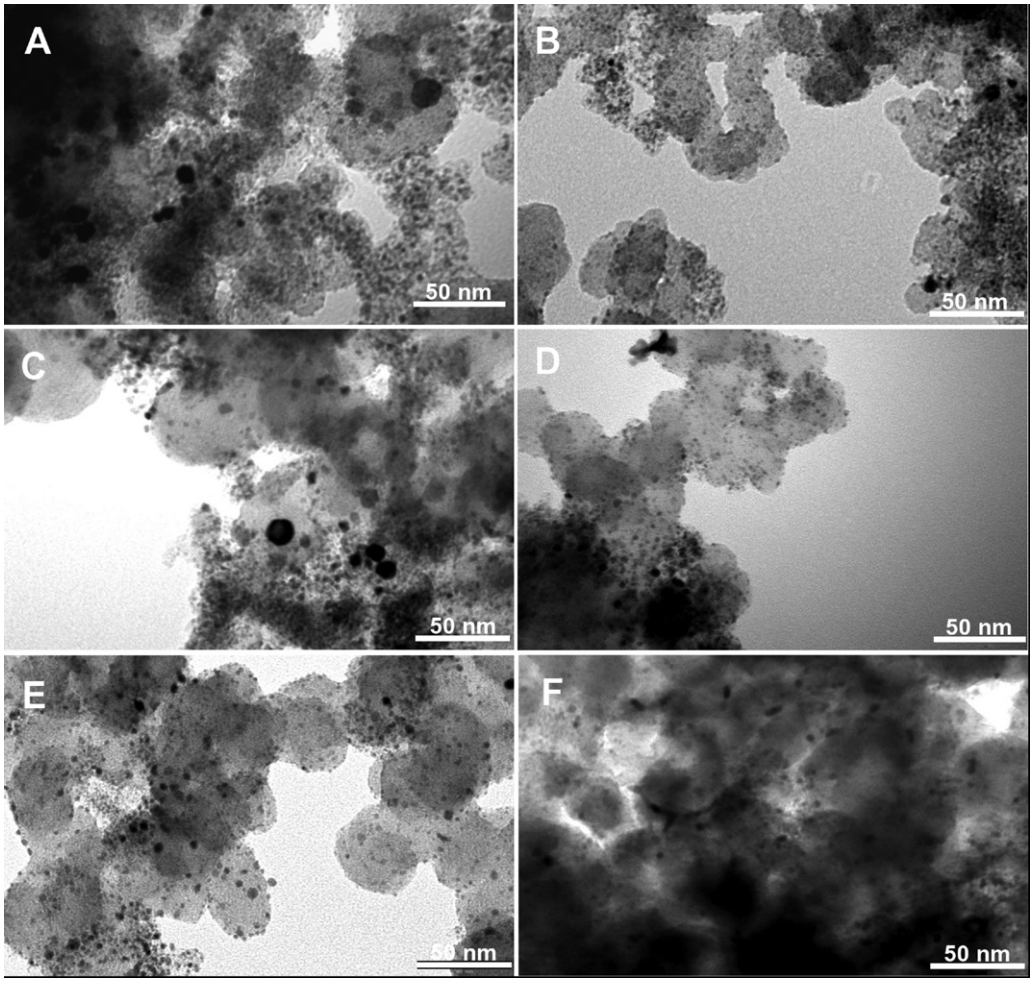

Fig. 1. TEM images of the Pt–Pd/C samples. All samples contain ca. 20% (by weight) of metal. Pt:Pd ratio was determined by XPS and is given in atomic percent. Sample A contain 0:100% Pt:Pd, B – 17:83% Pt:Pd, C – 28:72% Pt:Pd, D – 47:53% Pt:Pd, E – 71:29% Pt:Pd, F – 100:0% Pt:Pd.

2. Experimental

All chemicals were of analytical grade and were used without further purification. MilliQ (18 MΩ cm) water was used in preparation of electrolytes for electrochemical experiments and ethanol solution. High purity (N5.2) gases from Air Products Inc. (Poland) were used to deaerate ethanol solutions (Ar) and as a cathode gas (O_2).

2.1. Catalyst preparation

Carbon support (Vulcan XC-72R from Cabot Corporation, Boston, MA, USA) has been first subjected to the solution containing H_2O, 35% HCl_{aq} and 65% HNO_3 in 1:1:1 ratio (by volume) for at least 24 h, washed with ultrapure water, divided into pre-weighted samples and placed in quartz crucibles. One sample has been placed in air atmosphere at 100 °C for 1 h in order to estimate the water content. Subsequently, the water solution of $H_2PtCl_6{\cdot}6H_2O$ and $PdCl_2$ in 1 mol dm^{-3} HCl has been added in certain amounts to obtain the desired Pt:Pd ratio, and the sample was left overnight. The following day, sample was placed in a tube furnace in argon atmosphere and heated to 150 °C for 30 min. Subsequently the argon has been replaced with mixture of hydrogen and argon (1% of H_2 in Ar) and the constant flow was maintained for 160 min, when pure argon has been introduced again, and the sample was left to cool down.

2.2. Electrochemical investigation

Approximately 4.5 mg of each catalyst was added to the solution containing 280 μL of water, 200 μL of ethanol and 20 μL of 5% solution of Nafion® in ethanol and stirred until uniform suspension was formed. About 10 μL of the resulting suspension was placed on a gold disk (area ca. 10 mm^2), left to dry, and used as a working electrode in electrochemical experiments. Cyclic voltammetry experiments were performed in both: (a) 0.5 mol dm^{-3} pure sulfuric acid as well as (b) 0.5 mol dm^{-3} sulfuric acid in 0.5 mol dm^{-3} ethanol solutions. Chronoamperometric experiments were performed in 0.5 mol dm^{-3} ethanol solution in 0.5 mol dm^{-3} sulfuric acid. For electrochemical experiments PINE Instrument AFRDE5 bipotentiostat was used and data were collected using National Instruments NI USB-6211 data acquisition card. All potentials has been registered versus Hg/Hg_2SO_4/0.5 mol dm^{-3} H_2SO_4 reference electrode and later recalculated versus RHE.

2.3. Fuel cell experiments

To prepare membrane-electrode assemblies (MEAs), Nafion® 117 membrane (DuPoint) was first subjected to boiling in 0.5 mol dm^{-3} sulfuric acid for at least 3 h. Afterwards, the membrane was painted in the center with the obtained anode catalyst on one side, and 40% Pt/C (BASF/ETEK) on the other side as cathode, to obtain 10 cm^2 active area, reflecting the geometry of fuel cell hardware used. Loading of anode and cathode side was approximately 1 mg (metal) cm^{-2}. Amount of Nafion was adjusted to obtain ca. 30% in dry mass. When dry, each side had been covered with pre-cut carbon paper squares (Toray) to act as distribution layers and hot-pressed for 5 min. Fuel cell hardware from Fuel Cell Technologies Inc. was used. It consisted of two graphite plates with single serpentine flow pattern (10 cm^2 active area) and associated auxiliaries. The flow of oxygen at cathode side was maintained at 15 scm^3 s^{-1} using a mass flow controller from Sierra Instruments. Fuel (0.2 mol dm^{-3} of ethanol in water) was fed using a peristaltic pump at approximately 1 cm^3 min^{-1} rate. Ethanol solution was constantly deaerated (using Ar gas), prior and during introduction to the anode compartment of the fuel cell, to avoid the possible oxidation of ethanol (or acetaldehyde) at anode catalyst's surface by oxygen dissolved from air. Cell voltage and current were controlled using EG&G Princeton Applied Research 362 Scanning Potentiostat. As a rule, the fuel cell was stabilized for at least 2 h before starting the experiments and at least 30 min following the fuel cell voltage/discharge current change.

Products of ethanol oxidation were sampled from the port, located directly at the anode outlet, then introduced to Hewlett Packard 5890 Series II Gas Chromatograph (GC), which allowed for separation and qualitative and quantitative determination of the components of the mixture leaving fuel cell. For qualitative determination a Hewlett Packard 5971A Mass Selective Detector (MSD) was used, where for quantitative analysis a flame ionization detector (FID) was used. FID signal was calibrated for acetaldehyde and acetic acid in 0–5 molar percent range using ethanol as internal standard [42]. Data have been corrected for the amount of acetaldehyde and acetic acid produced due to oxygen permeation by subtraction the amounts obtained in currentless conditions [43]. Amount of CO_2 has been calculated from charge balance using the registered concentration of acetic acid and acetaldehyde and the fuel flow rate [43].

2.4. Morphology and composition analysis

Transmission electron microscopy (TEM) imaging and energy-dispersive X-ray spectroscopy (EDS) analysis were performed using electron microscope JEM 1400 (JEOL Co., Japan, 2008) equipped with energy-dispersive full range X-ray microanalysis system (EDS INCA Energy TEM, Oxford Instruments, Great Britain), tomographic holder and high resolution digital camera (CCD MORADA, SiS-Olympus, Germany).

An inductively coupled plasma mass spectrometer (ICP-MS) SCIEX "Elan 6100 DRC", Perkin-Elmer, was used for quantitative determination of platinum and palladium. The following ICP-MS operating parameters were used: radio frequency generator, 1100 W; lenses voltage, 7 V; nebulizer gas flow, 0.98 L min^{-1}; plasma gas flow, 15 L min^{-1}; dwell time, 0.1 s.

X-ray photoelectron spectroscopy (XPS) experiments were performed at Department of Physics, Silesia University, Katowice, Poland. PHI5700 spectrometer, made by Physical Electronics Inc. (PHI) has been employed. Monochromatized X-ray $Al_{K\alpha}$ radiation of energy equal to 1486 eV has been used. Spectra were recorded with 23.50 eV pass energy, 0.100 eV step and 100 ms dwell time. The measurements were performed in a vacuum of 10^{-10} Torr.

3. Results and discussion

3.1. Sample synthesis and morphology

The Pt–Pd/C samples obtained were characterized in regards of size and composition. TEM micrographs are presented in Fig. 1. It can be seen that the Pt–Pd nanoparticles are in sub-10 nm range. It has been reported, that in case of Pt–Pd nanoparticles synthesized using the same method the size increased from 3 to 5–8 nm as Pd concentration increased [44–47]. In our case we can expect the same behavior, and our images confirm the sub-10 nm size overall.

To determine the real composition, and to address the possible surface segregation, the composition of the samples was determined using ICP-MS after dissolution of the samples in *aqua regia* and using EDS and XPS. Those data are in good agreement, especially the data obtained using EDS and ICP-MS are within a few percent in the whole concentration range. The relationship between amount of Pt, determined from XPS (N_{XPS}) and ICP-MS (N_{ICPMS}) can be described using linear equation: $N_{XPS} = 1.02 \times N_{ICPMS}$, with $R^2 = 0.993$. The sample of the lowest Pt content shows a small deviation toward Pd-enriched surface, in

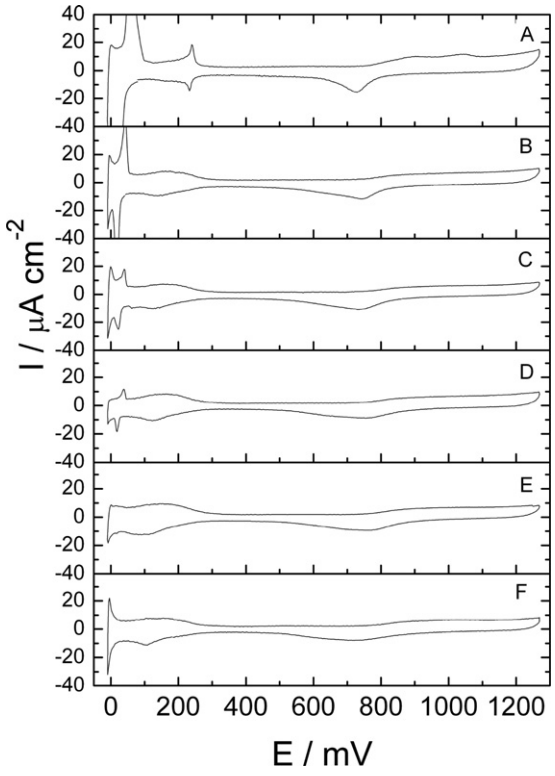

Fig. 2. Typical voltammograms for carbon-supported Pt–Pd nanoparticles in 0.5 mol dm^{-3} H_2SO_4. Scan rate: 5 mV s^{-1}. Surface normalized using charge associated with oxide reduction (320 μC cm^{-2}).

agreement with literature data [47–49], but no strong conclusions about surface segregation can be drawn, as the photoelectron inelastic mean free path in such material is very close to the size of the nanoparticles [50].

The Pt contents, determined from XPS data, for samples A–F were equal to 0, 17, 28, 47, 71 and 100 at.%, respectively, and the letter assignment is used consequently along the text.

3.2. Electrochemical investigation

For all samples the cyclic voltammetry in pure supporting electrolyte (0.5 mol dm^{-3} H_2SO_4) has been performed. The results are presented in Figs. 2 and 3. It can be seen, that the CV evolves from one typical for pure Pd (Fig. 2A) to those typical for pure Pt (Fig. 2F). It is worth to note, that: (i) the peak associated with hydrogen adsorption is present on the pure Pd only (at ca. 250 mV, c.f. Figs. 2A, 3 curve A and inset in Fig. 3), (ii) the potential of peaks associated with hydrogen absorption (below 100 mV) is dependent on the composition (inset in Fig. 3) and (iii) the charge associated with hydrogen absorption decreases much faster, than the Pd content, i.e. it decreased by a factor of two between sample A (100 at.% Pd) and B (71 at.% Pd) (Fig. 3). The above mentioned phenomena have already been observed for Pt–Pd alloys, when hydrogen adsorption and absorption were studied for such materials [51–55]. Alloying of Pd changes the hydrogen adsorption and absorption properties due to resulting changes in the crystal lattice parameter and electronic properties [56,57]. Those observations confirm that the samples prepared are well alloyed, as if they were a mixture of Pt and Pd, a simple superposition of the Pt and Pd voltammograms would be observed.

Sample surface was normalized using charge associated with surface oxide reduction peak (which can bee seen on cathode scan, at approximately 700 mV versus RHE), using charge value of 320 μC cm^{-2}. The same samples were used later

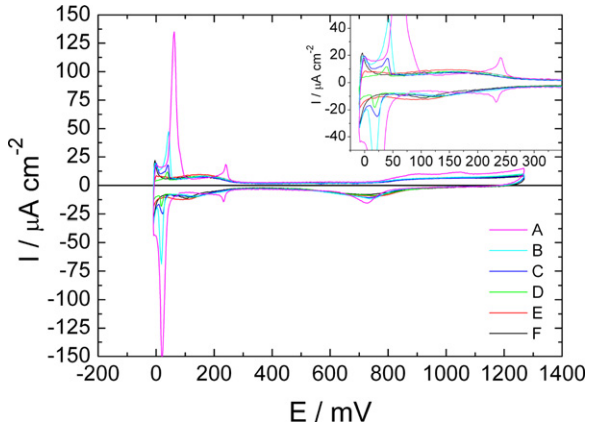

Fig. 3. Voltammograms registered for carbon-supported Pt–Pd nanoparticles in 0.5 mol dm^{-3} H_2SO_4/0.5 mol dm^{-3} ethanol. Scan rate: 5 mV s^{-1}. Surface normalized using charge associated with oxide reduction (320 μC cm^{-2}). Inset shows enlarged hydrogen region. Signals correlated to hydrogen adsorption/desorption are observed at ca. 250 mV in case of sample A (pure Pd) only. Signals due to hydrogen absorption/desorption are observed below 100 mV. It is worth to note, that the charge associated with those signals decrease more rapidly than Pd amounts, and also the change in the potential of hydrogen absorption/desorption as a function of concentration. This confirms that the samples are well alloyed.

to electrochemically oxidize ethanol during subsequent cyclic voltammetry experiments in 0.5 mol dm^{-3} ethanol in 0.5 mol dm^{-3} H_2SO_4 and the results are presented in Fig. 4. It can be seen, that pure Pt (Fig. 4F) is the most active in terms of both the onset potential of ethanol oxidation and the overall voltamperometric current. It is worth to note, that second sample in terms of activity is the sample which contains 47 at.% of Pt (Fig. 4D), and all the other samples (except totally inactive, pure Pd – Fig. 4A) are similar in terms of activity (both – the registered current and the onset potential). The relatively high activity of Pt–Pd with composition close to 1:1 for ethanol oxidation has been reported previously [6] and our observation correlates with the literature data [58]. This observation will be discussed in more details below.

Chronoamperometric experiments have been performed, for pulse time equal to 600 and 6 s in the potential range between 340 and 590 mV versus RHE, and the results are presented in Figs. 5 and 6. Open squares represent the registered current density per surface area, whereas filled circles represent the same current density, but recalculated per platinum surface only, as determined using XPS. It is worth mentioning that the relation between chronoamperometric current density and composition for all potentials and both experiment times follows the same

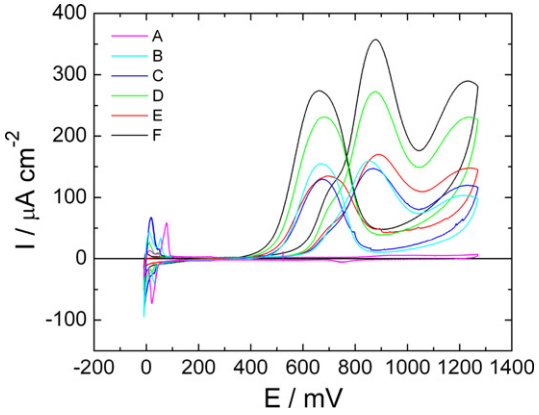

Fig. 4. Typical voltammograms for carbon-supported Pt–Pd nanoparticles in 0.5 mol dm^{-3} H_2SO_4/0.5 mol dm^{-3} ethanol. Scan rate: 5 mV s^{-1}. Surface normalized using charge associated with oxide reduction (320 μC cm^{-2}).

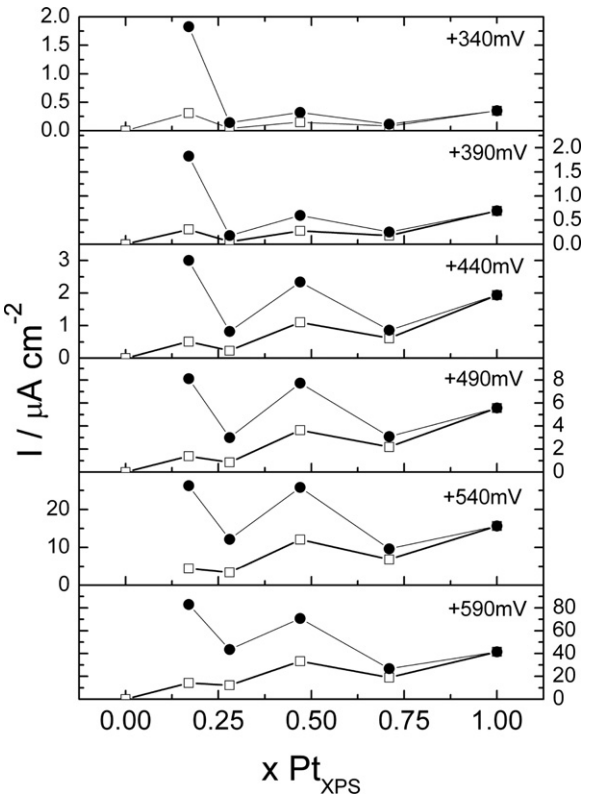

Fig. 5. Chronoamperometric current registered for carbon-supported Pt–Pd nanoparticles in 0.5 mol dm^{-3} H_2SO_4/0.5 mol dm^{-3} ethanol after 600 s. Number in right corner denotes the potential of working electrode used (versus RHE). Open squares represent the absolute current densities, where filled circles denote current densities recalculated per Pt surface.

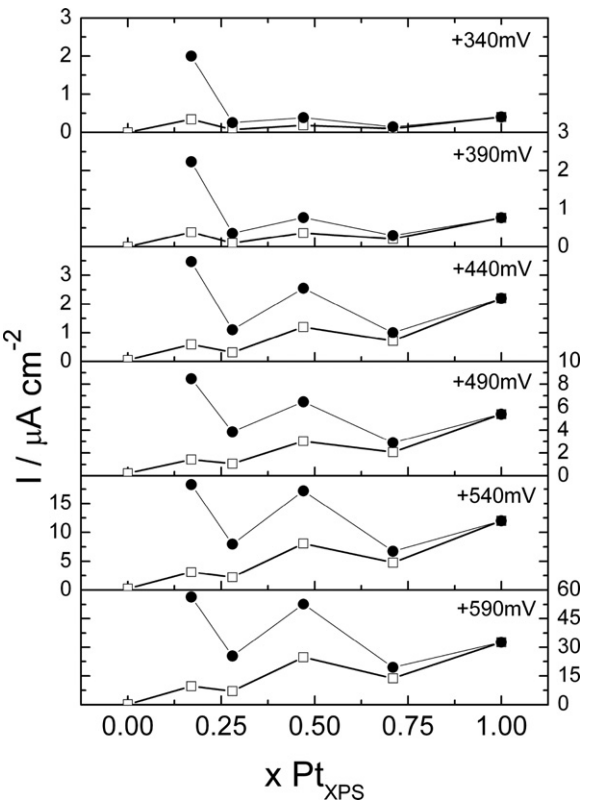

Fig. 6. Chronoamperometric current registered for carbon-supported Pt–Pd nanoparticles in 0.5 mol dm^{-3} H_2SO_4/0.5 mol dm^{-3} ethanol after 6 s. Number in right corner denotes the potential of working electrode used (versus RHE). Open squares represent the absolute current densities, where filled circles denote current densities recalculated per Pt surface.

pattern, decreasing almost linearly from those registered for pure Pt to zero for pure Pd, where two samples show a small increase of the chronoamperometric current above the linear overall decrease as Pt amount decrease: one is the sample consisting of 47 at.% of Pt, and the second is for the sample containing 17 at.% of Pt (Figs. 5 and 6). The small increase above the tendency of chronoamperometric current to linearly decrease as a function of Pt content, observed for 47 at.% of Pt is most probably a result of more pronounced bi-functional mechanism for that composition, as confirmed by fuel cell products analysis (see below). The another small increase above the same decreasing tendency of chronoamperometric current, observed at 17 at.% of Pt is the most pronounced for low electrode potential (340 mV versus RHE) and long experiment time (see Figs. 5 and 6). Those observations will be correlated to the observed fuel cell product distribution and discussed in the next section of this paper.

When the chronoamperometric current density is calculated per the area of Pt, the different pattern emerges: the current density increases slightly as the Pt content decreases. This shows that Pt becomes more active when it is diluted with Pd. The most active (relatively – per Pt surface) sample is the one with the lowest Pt content (sample B containing 17 at.% of Pt). The maximum at 47 at.% of Pt is still present, but less pronounced. We will discuss the possible explanation of this behavior in more details below.

3.3. *Product distribution and comments on mechanism of ethanol electrooxiadtion on Pt–Pd as determined from fuel cell experiments.*

Fuel cell experiments with those samples used as anodes let us to determine the product distribution when ethanol is oxidized in working fuel cell and to comment on the mechanism of that process. The overall activity follows the patterns observed using cyclic voltammetry and chronoamperometry, but the analysis of distribution of products suggests that the observed activity is a result of interplay between the changes of Pt activity when it is diluted with Pd, the role of bi-functional mechanism and the ensemble effect in that system. Namely, when amounts of products obtained in working fuel cell are plotted as a function of Pt content and cell voltage (Fig. 7) it can be observed that the overall amounts of products decrease as the Pt content decrease, with small local maximum in acetaldehyde and acetic acid production again at 47 at.% of Pt (see Fig. 7-1 and 7-2). This observation is in perfect agreement with the electrochemical data (Figs. 3–6) and most probably the local maximum in activity is correlated to increased acetic acid production due to the bi-functional mechanism, which should be most pronounced for the samples with composition close to 1:1 [6].

Additionally there is a small local maximum for CO_2 production for sample containing 17 at.% of Pt at low cell voltage (Fig. 7-3), which correlates to local maximum on chronoamperometric data (Figs. 5 and 6). It is worth to note that at this concentration CO_2 is the main product, as the amounts of acetaldehyde and acetic acid decrease sharply for Pt concentration lower than 28 at.% regardless of the cell voltage (Fig. 7-1 and 7-2). Also, on the chronoamperometric data the maximum for 17 at.% of Pt was the most pronounced for low electrode potential, which correlates to high cell voltages. If we assume the cathode potential of ca. 800 mV, then the 340 mV of anode corresponds to ca. 460 mV of cell voltage. At this condition the production of acetaldehyde and acetic acid is negligible (less than 1 mmol dm^{-2}, see Fig. 7-1–7-3), but the amount of CO_2 is ca. 2 mmol dm^{-2}. This suggests a direct patch of oxidation of ethanol to CO_2 at those conditions.

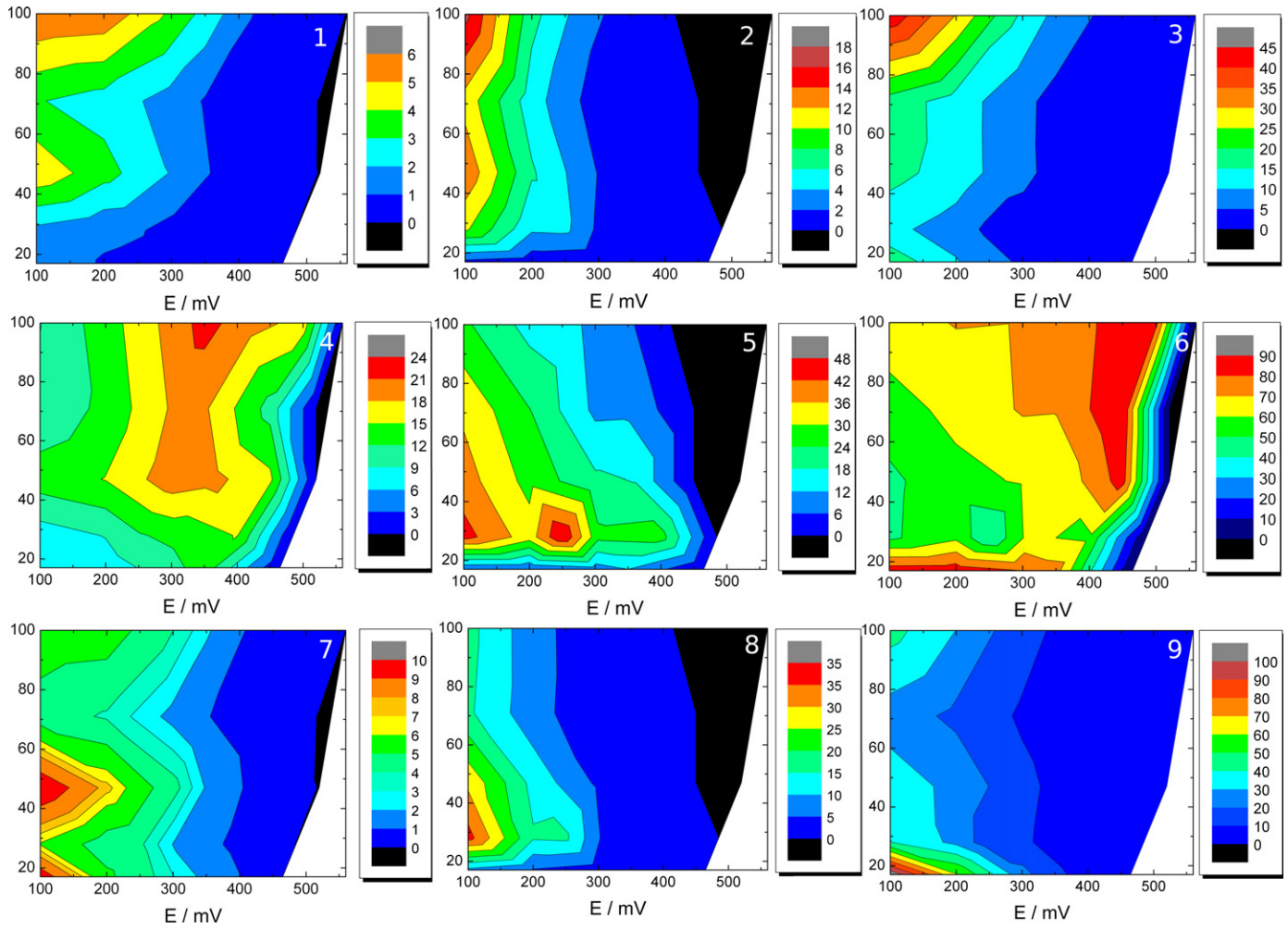

Fig. 7. Distribution of products of ethanol oxidation in working direct ethanol fuel cell. In all cases vertical axis denote Pt content in atomic percent, and the horizontal axis denotes cell voltage. Color scale represents the registered amounts in mol dm^{-3} (Figs. 1-3), percent (Figs. 4-6) or mol dm^{-3} per Pt surface (Figs. 7-9) (see text for more details). Numerical values corresponding to colors are given in legend at the right of each figure. Please note that different scales have been used to exaggerate the relationship between amount of products and cell voltage and catalyst's composition. All data presented for 90 °C cell temperature. 1. Acetaldehyde yield in mmol dm^{-3}, 2. Acetic acid yield in mmol dm^{-2}, 3. CO_2 yield in mmol dm^{-3}, 4. Relative amount of acetaldehyde in molar percent, 5. Relative amount of acetic acid in molar percent, 6. Relative amount of CO_2 in molar percent, 7. Amount of acetaldehyde produced per Pt surface in mmol dm^{-3}, 8. Amount of acetic acid produced per Pt surface in mmol dm^{-3}, 9. Amount of CO_2 produced per Pt surface in mmol dm^{-3}.

From the product analysis it can be also determined, that the absolute amount of acetic acid is correlated mainly to the cell voltage (Fig. 7-2) for Pt amount ≥28 at.%, where acetaldehyde and CO_2 are produced in significant amounts for certain composition and at relatively narrow range of cell voltages (Fig. 7-1 and 7-3, respectively). Particularly, the amount of acetic acid for given cell voltage is almost constant when Pt amount is ≥28 at.% (with a small deviation at composition close to 1:1), regardless of surface composition. This suggests relatively small activity of palladium in activating water, and minor role of the bi-functional mechanism in the overall activity of Pt–Pd alloys. This can be compared to the known properties of Pt–Sn and Pt–Ru alloys which are very active toward electrooxidation of ethanol mainly due to the bi-functional mechanism, which results in acetic acid being the most important product, reaching more than 50% in case of Pt–Ru and more than 90% in case of Pt–Sn [43].

Additional insight on acetic acid production on fuel cell catalysts comes from work of Wieckowski [59] and independently Behm [60], who used sophisticated spectroscopic techniques (broadband sum-frequency generation and electrochemical attenuated total reflection, respectively) to investigate ethanol electrooxidation on platinum. They shown that when Pt surface is poisoned by CO, ethanol cannot be oxidized to acetic acid. Only when Pt surface is freed from CO, the acetic acid production can be significant. Our observation correlates and extends those results, as at high cell voltages (which are correlated to low anode potential) the adsorbed CO cannot be effectively oxidized. But at the low cell voltages (high anode potentials) the CO oxidation process can occur, which is observed as increased CO_2 and acetic acid production. It is important to note, that the presence of Pd does not significantly change the properties of Pt in that respect, as opposed to, for instance, Pt–Ru and Pt–Sn.

If we focus on acetaldehyde and CO_2 production, it can be seen, that those compounds are evident mostly at low cell voltages and high Pt content (see Fig. 7-1 and 7-3, respectively). From those data it can be concluded, that: (i) the decrease in ethanol electrooxidation current when Pt amount decrease (as seen on chronoamperograms, Figs. 5 and 6) can be correlated to decreased production of CO_2 and to the much less extend, decreased production of acetaldehyde, as the amount of acetic acid remains constant, (ii) certain surface composition and anode potential are necessary for production of those two compounds, which is especially pronounced in case of CO_2 and (iii) at low cell voltages production of CO_2 dominates, as the adsorbed CO can be oxidized to CO_2, which

results in production of CO_2 at least at 20 mmol dm^{-3} level, with local maximum at over 40 mmol dm^{-3} in case of pure Pt and 100 mV cell voltage. This can be compared to ca. 2-3 mmol dm^{-3} in case of acetaldehyde and usually less than 20 mmol dm^{-3} for acetic acid.

The relative amounts of acetaldehyde, acetic acid and CO_2 are calculated to comment on relationship between acetaldehyde, acetic acid and CO_2 in conditions where turnover frequency factor is minimized. Such data are presented in Fig. 7-4, 7-5 and 7-6. It can be seen, that amount of acetic acid has a well pronounced maximum at low cell voltage and Pt content between 40 and 20 at.%. This is another confirmation of the role of bi-functional mechanism in the overall activity toward ethanol electrooxidation of Pt–Pd nanoparticles with Pt:Pd ratio close to 1:1. Significant acetaldehyde amounts are centered at ca. 350 mV for samples containing more than 40 at.% of Pt, and is generally independent of acetic acid and CO_2 production. The acetaldehyde production is generally the lowest, reaching 20 molar percent, as compared to acetic acid (up to 50 molar percent) and CO_2 (up to 90 molar percent). Electrooxidation of ethanol on Pt has been extensively studied, and it is generally accepted, that ethanol electrooxidation to acetic acid occurs mainly at high electrode potentials (low cell voltages), where water can be effectively activated to form oxygenated species, where at low electrode potentials (high cell voltage) acetaldehyde is the main product. It can be seen from our data, that the overall scheme is still valid for the Pt–Pd systems.

From the plots of the relative amounts of acetic acid and CO_2 (Fig. 7-5 and 7-6) the new relationship between acetic acid and CO_2 emerges – the maxima of CO_2 production correlate with minima of acetic acid production and vice versa. To some extend it is caused by the presentation method, as those results are relative one to another and those two are the main components. This is especially true for high cell voltage where the overall amounts of any products are small. But the overall tendency can be also understood in terms of changes in the possible ethanol electrooxidation reaction patch. Production of acetaldehyde is a simple dehydrogenation process, where for acetic acid some form of oxygenated species is required (usually assumed to be surface OH groups). It is clear from the data presented here (Fig. 7-4–7-6), that the dehydrogenation process can occur at much lower cell voltages, where surface of catalyst is covered by CO. But as long as CO is present on the surface, the acetic acid cannot be produced [59,60]. Thus the relationship between the amount of CO_2 and acetic acid can be understood in terms of competition for catalyst's surface between CO and water or other weakly bonded oxygenated species, as CO bonds to the surface of Pt so strongly, that it can displace virtually any other component, which may be present on the surface.

It is worth to note, that the observed relative amount of CO_2 (Fig. 7-6) is higher than usually reported for other Pt-containing systems [5,16,17,24,30,32,33,35], which makes Pt–Pd alloys a very interesting system to further study from the mechanistic point of view. For some conditions it can reach 90%, which has not been reported previously. But it must be remembered that such high relative CO_2 production occurs in conditions where the overall current density is close to zero. The reason why such high concentration has not been observed previously is partially due to the fact, that previous results were not corrected for oxygen permeation, which results in high observed background amounts of acetaldehyde and acetic acid [43], thus lowering the relative amount of CO_2. High CO_2 yield is observed in situations where registered current is rather low, thus the relative amounts of products due to parasitic chemical oxidation of ethanol by permeating oxygen are high, resulting in significant distortion in the literature data. The overall catalytic activity in such conditions is low, but it is an important observation from mechanistic point of view and also it stresses the need for correction for parasitic processes occurring in the working fuel cell.

To investigate the change of activity of Pt sites when Pt is alloyed with Pd and the role of ensemble effect and possible changes in electronic properties, the relative amounts of ethanol oxidation products were re-calculated per Pt surface (Figs. 7-7–7-9). It can be seen, that the relationship between Pt activity and concentration is non-linear. The acetaldehyde production per Pt site increases as Pt amount decreases in the whole concentration range, with two local maxima: at 47 and 17 at. % of Pt. Production of acetic acid is centered at Pt:Pd ratio close to 1:1, but CO_2 is produced in significant amount for the samples with low Pt contents only. The maxima of relative amounts of acetic acid and CO_2 correlate with the overall local maxima on the chronoamperometric data (Figs. 5 and 6) and the combined product distribution correlates with the overall slight increase in activity of Pt atoms when Pt amount decrease (Figs. 5 and 6, filled symbols). Increased production of acetic acid for Pt:Pd ratio close to 1:1 has already been discussed. Increased amount of CO_2 per Pt amount observed when Pt amount decreases can be explained based on the so-called ensemble effect. Namely, when Pt contents become low, the probability of presence of Pt clusters containing 2- or 3-Pt atoms also decreases. Those clusters are required for adsorption of ethanol parallel to the surface, as ethanol does not adsorb on palladium. Thus in conditions, where Pt concentration is low, ethanol molecule can only adsorb perpendicularly to the surface. We postulate, based on results presented in Fig. 7-7–7-9, in that orientation, dehydrogentation reaction can occur, leading to acetaldehyde (Fig. 7-7), or linearly bonded CO, which can be later oxidized to CO_2 (Fig. 7–9), but no acetic acid can be produced (Fig. 7-8). Obviously for acetic acid production, substrate, or some intermediate form, must be adsorbed parallel to the surface of catalyst, and when such mode is not possible, the whole branch stops. The role of electronic factors, being a result of Pt–Pd interactions, both due to the geometry change and charge transfer cannot also be excluded. This is currently under detailed examination in our laboratory.

4. Conclusions

We have presented here the relation between amounts of products of ethanol electrooxidation in working, low temperature fuel cell. We also presented a correlation between ex situ electrochemical and fuel cell product analysis data regarding ethanol oxidation on Pt–Pd nanoparticles of different compositions. Such data allowed us to comment on the interplay between the bi-functional mechanism and geometry factors, influencing the catalytic activity, when Pt is diluted by Pd. The bi-functional mechanism can be observed mainly for the nanoparticles with the relative Pt to Pd amount close to 1:1, where relative amounts of acetic acid are the highest. Respectively, when Pt contents becomes small, there is significant contribution from the geometry or electronic factors, or both, which inhibits production of acetic acid and results in increased production of acetaldehyde and CO_2.

Acknowledgements

The support from Ministry of Science and Higher Education (Poland) under the grant N N204 527739 is appreciated. The TEM and EDS studies were performed at the Laboratory of Electron Microscopy, Nencki Institute of Experimental Biology, Warsaw, Poland. The TEM equipment was installed within the project sponsored by the EU Structural Funds: Centre of Advanced Technology BIM – equipment purchase for the Laboratory of Biological and Medical Imaging. We thank Dr. Joanna Kowalska for performing the ICP-MS analysis. We are also indebted to Prof. Dr. hab. Jacek Szade, Dr. Antoni Winiarski, Dr. Marek Kulpa and mgr Michał Pilch

from Department of Physics, Silesia University, Katowice, Poland for helpful discussion and registering the XP spectra.

References

[1] J.H. Wee, Renewable & Sustainable Energy Reviews 11 (2007) 1720–1738.
[2] C. Lamy, A. Lima, V. LeRhun, F. Delime, C. Coutanceau, J.M. Leger, Journal of Power Sources 105 (2002) 283–296.
[3] A.S. Arico, S. Srinivasan, V. Antonucci, Fuel Cells 1 (2001) 133–161.
[4] F. Delime, J.M. Leger, C. Lamy, Journal of Applied Electrochemistry 29 (1999) 1249–1254.
[5] C. Lamy, E.M. Belgsir, J.M. Leger, Journal of Applied Electrochemistry 31 (2001) 799–809.
[6] W.J. Zhou, Z.H. Zhou, S.Q. Song, W.Z. Li, G.Q. Sun, P. Tsiakaras, Q. Xin, Applied Catalysis B: Environmental 46 (2003) 273–285.
[7] W.J. Zhou, W.Z. Li, S.Q. Song, Z.H. Zhou, L.H. Jiang, G.Q. Sun, Q. Xin, K. Poulianitis, S. Kontou, P. Tsiakaras, Journal of Power Sources 131 (2004) 217–223.
[8] W.J. Zhou, S.Q. Song, W.Z. Li, G.Q. Sun, Q. Xin, S. Kontou, K. Poulianitis, P. Tsiakaras, Solid State Ionics 175 (2004) 797–803.
[9] W.J. Zhou, B. Zhou, W.Z. Li, Z.H. Zhou, S.Q. Song, G.Q. Sun, Q. Xin, S. Douvartzides, A. Goula, P. Tsiakaras, Journal of Power Sources 126 (2004) 16–22.
[10] J.M. Leger, S. Rousseau, C. Coutanceau, F. Hahn, C. Lamy, Electrochimica Acta 50 (2005) 5118–5125.
[11] S.Q. Song, W.J. Zhou, Z.H. Zhou, L.H. Jiang, G.Q. Sun, Q. Xin, V. Leontidis, S. Kontou, P. Tsiakaras, International Journal of Hydrogen Energy 30 (2005) 995–1001.
[12] L. Colmenares, H. Wang, Z. Jusys, L. Jiang, S. Yan, G.Q. Sun, R.J. Behm, Electrochimica Acta 52 (2006) 221–233.
[13] F. Vigier, S. Rousseau, C. Coutanceau, J.M. Leger, C. Lamy, Topics in Catalysis 40 (2006) 111–121.
[14] H. Wang, Z. Jusys, R.J. Behm, Journal of Power Sources 154 (2006) 351–359.
[15] P.E. Tsiakaras, Journal of Power Sources 171 (2007) 107–112.
[16] A. Kowal, M. Li, M. Shao, K. Sasaki, M.B. Vukmirovic, J. Zhang, N.S. Marinkovic, P. Liu, A.I. Frenkel, R.R. Adzic, Nature Materials 8 (2009) 325–330.
[17] M. Li, A. Kowal, K. Sasaki, N. Marinkovic, D. Su, E. Korach, P. Liu, R.R. Adzic, Electrochimica Acta 55 (2010) 4331–4338.
[18] A.S. Arico, P. Creti, P.L. Antonucci, V. Antonucci, Electrochemical and Solid-State Letters 1 (1998) 66–68.
[19] J.T. Wang, S. Wasmus, R.F. Savinell, Journal of the Electrochemical Society 142 (1995) 4218–4224.
[20] T. Iwasita, R. Dalbeck, E. Pastor, X. Xia, Electrochimica Acta 39 (1994) 1817–1823.
[21] M. Watanabe, S. Motoo, Journal of Electroanalytical Chemistry 60 (1975) 267–273.
[22] H. Wang, Z. Jusys, R.J. Behm, Journal of Physical Chemistry B 108 (2004) 19413–19424.
[23] J.P.I. de Souza, S.L. Queiroz, K. Bergamaski, E.R. Gonzalez, F.C. Nart, Journal of Physical Chemistry B 106 (2002) 9825–9830.
[24] F. Vigier, C. Coutanceau, F. Hahn, E.M. Belgsir, C. Lamy, Journal of Electroanalytical Chemistry 563 (2004) 81–89.
[25] D.M. dos Anjos, F. Hahn, J.M. Leger, K.B. Kokoh, G. Tremiliosi, Journal of the Brazilian Chemical Society 19 (2008) 795–802.
[26] E. Antolini, F. Colmati, E.R. Gonzalez, Journal of Power Sources 193 (2009) 555–561.
[27] A. Czerwinski, M.S. Soszko, M.M. Lukaszewski, Z. Mianowska, Journal of Power Sources 196 (2011) 3513–3522.
[28] A. Czerwinski, W. Tokarz, H. Siwek, P. Piela, Electrochimica Acta 52 (2007) 5565–5573.
[29] B. Bittins-Cattaneo, S. Wilhelm, E. Cattaneo, H.W. Buschmann, W. Vielstich, Berichte Der Bunsen-Gesellschaft: Physical Chemistry Chemical Physics 92 (1988) 1210–1218.
[30] K. Taneda, T. Taniyama, Y. Yamazaki, Electrochemistry 72 (2004) 700–702.
[31] S. Rousseau, C. Coutanceau, C. Lamy, J.M. Leger, Journal of Power Sources 158 (2006) 18–24.
[32] D.D. James, D.V. Bennett, G.C. Li, A. Ghumman, R.J. Helleur, P.G. Pickup, Electrochemistry Communications 11 (2009) 1877–1880.
[33] G. Andreadis, V. Stergiopoulos, S. Song, P. Tsiakaras, Applied Catalysis B: Environmental 100 (2010) 157–164.
[34] D.D. James, P.G. Pickup, Electrochimica Acta 55 (2010) 3824–3829.
[35] P. Tsiakaras, G. Andreadis, V. Stergiopoulos, S. Song, Applied Catalysis B: Environmental 100 (2010) 157–164.
[36] H. Hitmi, E.M. Belgsir, J.M. Leger, C. Lamy, R.O. Lezna, Electrochimica Acta 39 (1994) 407–415.
[37] E. Antolini, Journal of Power Sources 170 (2007) 1–12.
[38] R. Alcala, J.W. Shabaker, G.W. Huber, M.A. Sanchez-Castillo, J.A. Dumesic, Journal of Physical Chemistry B 109 (2005) 2074–2085.
[39] H.A. Gasteiger, N. Markovic, P.N. Ross, E.J. Cairns, Electrochimica Acta 39 (1994) 1825–1832.
[40] E. Antolini, Energy & Environmental Science 2 (2009) 915–931.
[41] E. Antolini, S.C. Zignani, S.F. Santos, E.R. Gonzalez, Electrochimica Acta 56 (2011) 2299–2305.
[42] S.V. Cherepitsa, S.M. Bychkov, A.N. Kovalenko, A.L. Mazanik, N.M. Selemina, O.B. Seredinskaya, Journal of Analytical Chemistry 58 (2003) 368–371.
[43] A. Jablonski, P.J. Kulesza, A. Lewera, Journal of Power Sources 196 (2011) 4714–4718.
[44] H. Li, G. Sun, N. Li, S. Sun, D. Su, Q. Xin, The Journal of Physical Chemistry C 111 (2007) 5605–5617.
[45] A.C. Garcia, V.A. Paganin, E.A. Ticianelli, Electrochimica Acta 53 (2008) 4309–4315.
[46] W. Wang, Q. Huang, J. Liu, Z. Zou, Z. Li, H. Yang, Electrochemistry Communications 10 (2008) 1396–1399.
[47] J. Yang, J.Y. Lee, Q. Zhang, W. Zhou, Z. Liu, Journal of the Electrochemical Society 155 (2008) B776–B781.
[48] J.L. Rousset, A.J. Renouprez, A.M. Cadrot, Physical Review B 58 (1998) 2150.
[49] C. Massen, T.V. Mortimer-Jones, R.L. Johnston, Journal of the Chemical Society, Dalton Transactions (2002) 4375–4388.
[50] D. Briggs, in: J.T. Grant (Ed.), Surface Analysis by Auger and X-ray Photoelectron Spectroscopy, IM Publications and Surface Spectra Limited, Chichester, Manchester, UK, 2003.
[51] K. Hubkowska, M. Lukaszewski, A. Czerwinski, Electrochimica Acta 56 (2010) 235–242.
[52] K. Hubkowska, M. Lukaszewski, A. Czerwinski, Electrochimica Acta 56 (2011) 2344–2350.
[53] M. Lukaszewski, K. Hubkowska, A. Czerwinski, Physical Chemistry Chemical Physics 12 (2010) 14567–14572.
[54] M. Lukaszewski, K. Hubkowska, A. Czerwinski, Przemysl Chemiczny 90 (2011) 1201–1206.
[55] M. Lukaszewski, K. Hubkowska, A. Czerwinski, Journal of Electroanalytical Chemistry 651 (2011) 131–142.
[56] X.Z. Ke, G.J. Kramer, O.M. Lovvik, Journal of Physics: Condensed Matter 16 (2004) 6267–6277.
[57] L.A. Kibler, A.M. El-Aziz, R. Hoyer, D.M. Kolb, Angewandte Chemie: International Edition 44 (2005) 2080–2084.
[58] T. Lopes, E. Antolini, E.R. Gonzalez, International Journal of Hydrogen Energy 33 (2008) 5563–5570.
[59] A. Wieckowski, R.B. Kutz, B. Braunschweig, P. Mukherjee, R.L. Behrens, D.D. Dlott, Journal of Catalysis 278 (2011) 181–188.
[60] M. Heinen, Z. Jusys, R.J. Behm, Journal of Physical Chemistry C 114 (2010) 9850–9864.